communications materials

Article

https://doi.org/10.1038/s43246-025-00733-2

Direct observation of Mn-ion dissolution from $LiMn_2O_4$ lithium battery cathode to electrolyte

Nithya Hellar[1,2] ✉, Yoshiki Iwai[1,3], Masato Ohzu[1], Sebastian Brox[4], Arunkumar Dorai[1], Reiji Takekawa[1], Naoaki Kuwata[1,5], Junichi Kawamura[1] ✉ & Martin Winter[4,6]

The degradation of lithium-ion batteries has become a concerning issue. One problem is metal ion dissolution from the cathode material, such as Mn^{2+} dissolution from spinel-type $LiMn_2O_4$ (LMO). However, direct observation of the dissolution process has yet to be reported. Here, we establish in-situ ^1H nuclear magnetic resonance imaging (MRI) measurement as an efficient technique to observe Mn^{2+} dissolution from a model lithium battery with LMO as the cathode. We observe an increase in the MRI signal intensity near the cathode, confirming the dissolution of Mn^{2+} from the cathode to the electrolyte. Moreover, we show that Mn^{2+} dissolution from LMO can be suppressed using an appropriate choice of electrolytes. We believe the method developed here can answer the long-time unanswered question of when, where, and how the metal ion dissolution occurs in the lithium-ion battery electrode and can be extended to other electrochemical systems.

Spinel-type LMO and its derivatives are promising cathode materials for the development of batteries suitable for electric vehicles due to their high operating voltage, low cost, and safe performance[1]. Although LMO operates at high voltage, it has its own disadvantage of structural instability and capacity fading when operated at potentials >4.3 V. The reason for capacity fading is (i) electrolyte decomposition when operated at high potential, (ii) phase change (Jahn-Teller distortion/structural instability), and (iii) dissolution of manganese (Mn) to the electrolyte through hunter's disproportionation reaction [$2Mn^{3+}(s) \rightarrow Mn^{4+}(s) + Mn^{2+}(l)$][2–4]. Among these, active metal dissolution (Mn) is the most serious problem for long-time applications such as electric vehicles and smart grid applications, where slow deterioration of battery performance causes maintenance problems and increases the lifetime cost.

For over a decade, several reports were published on different methods to suppress Mn dissolution and develop a highly stable LMO. Also, few reports are found that quantitatively measure dissoluted Mn ion concentration in the electrolyte[5–10]. To understand the metal ion dissolution, it is important to detect when, where, and how much the dissolution happens in the lithium batteries. Therefore, developing a new analytical technique sensitive to the metal ions in electrode materials of battery systems is warranted. Moreover, developing in-situ techniques will help in future efforts to improve battery design and performance.

Nuclear magnetic resonance imaging (MRI) is a non-invasive technique, which combines spectroscopy and imaging, makes it a powerful tool and is widely used in various applications such as batteries, fuel cells, corrosion cells, and metallurgy[11–20]. However, no reports have focused on identifying the metal ion dissolution in lithium batteries using in-situ MRI [see Supplementary Table 1 for past reports on application of MRI in battery research]. Also, our group first reported that proton (^1H) MRI is a suitable technique to visualize the degradation of battery electrolytes in a model lithium battery[21]. In the present work, we demonstrate the direct observation and quantification of Mn ion dissolution from LMO cathode using in-situ ^1H MRI. Further, we identified an electrolyte system that suppresses the metal ion dissolution from LMO.

[1]Institute of Multidisciplinary Research for Advanced Materials (IMRAM), Tohoku University, 2-1-1 Katahira, Aoba-ku, Sendai, 980-8577, Japan. [2]New Industry Creation Hatchery Center (NICHe), Tohoku University, 2-1-1 Katahira, Aoba-ku, Sendai, 980-8577, Japan. [3]Technology and Innovation Division, Panasonic Corporation, 3-1-1 Yagumo-naka-machi, Moriguchi City, Osaka, 570-8501, Japan. [4]MEET Battery Research Center, Institute of Physical Chemistry, University of Münster, Corrensstraße 46, 48149 Münster, Germany. [5]Research Center for Energy and Environmental Materials, National Institute of Materials Science (NIMS), 1-1 Namiki, Tsukuba, Ibaraki, 305-0044, Japan. [6]Helmholtz Institute Münster (IEK-12), Forschungszentrum Jülich GmbH, Corrensstraße 46, 48149 Münster, Germany. ✉e-mail: hellar.nithya.e4@tohoku.ac.jp; junichi.kawamura.a8@tohoku.ac.jp

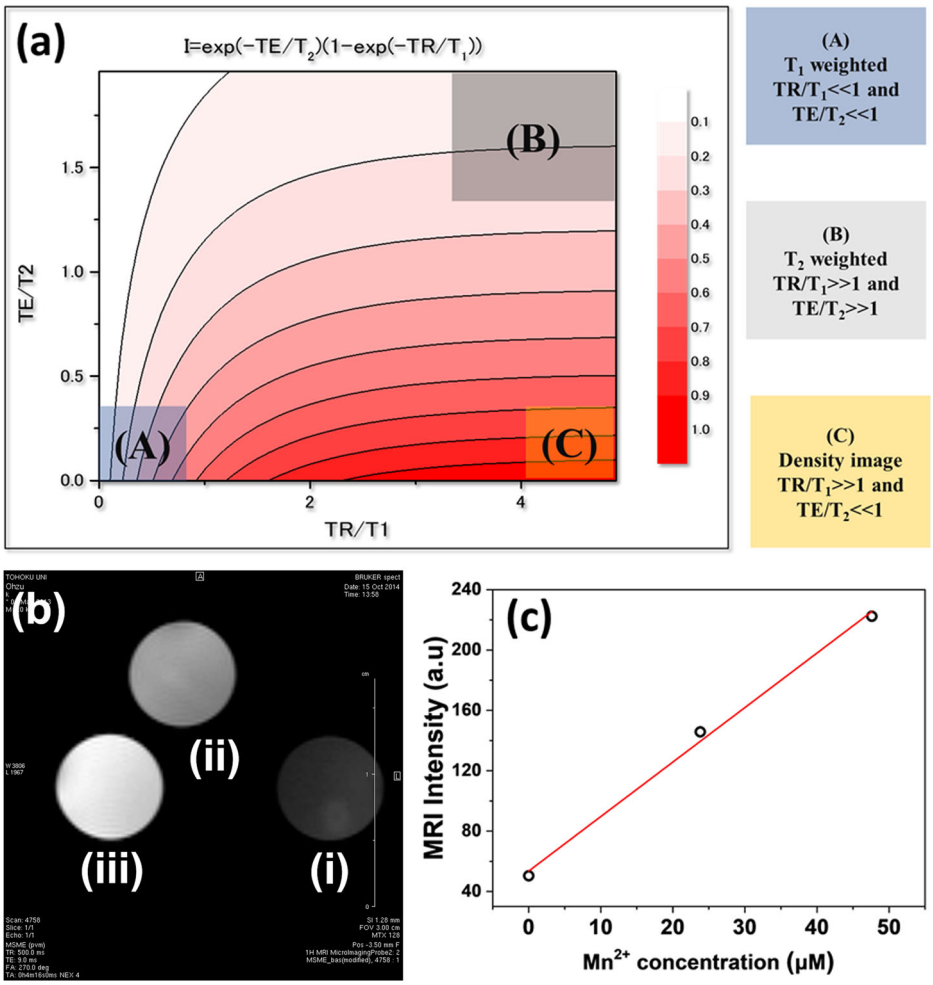

Fig. 1 | Evolution of MRI signal intensity. a MRI intensity change calculated according to Eq. 1, with respect to change in relaxation time, **b** MR images of standard $MnCl_2$ in 1 M $LiPF_6$ EC:DMC gel electrolyte (i) 0 (ii) 24 and (iii) 48 μM Mn^{2+}, **c** Mn^{2+} concentration dependence of average MRI signal intensity extracted from (**b**).

Results and discussion

Theory and scope of MRI in lithium battery electrolyte

In principle, the MRI signal intensity, when obtained using the spin-echo technique, is given by

$$I(x,y) \propto \rho_{(x,y)}\left\{1-\exp\left(\frac{-TR}{T_1}\right)\right\}\exp\left(\frac{-TE}{T_2}\right) \quad (1)$$

where TR and TE are repetition and echo time, which are experimental parameters. T_1 and T_2 are spin-lattice relaxation, and spin-spin relaxation time, which are material properties. Therefore, from Eq. 1, MRI signal intensity is clearly affected when T_1 and T_2 relaxation time changes. By varying the experimental parameters, we can obtain contrast-enhanced images that are either T_1 weighted (longitudinal relaxation), T_2 weighted (transverse relaxation), or proton density weighted images. A comparative image intensity plot generated by varying the parameters used in Eq. 1 is shown in Fig. 1a. However, there is no exact reference range. In this study, we have used the change in the relaxation time of the solvent protons in the electrolyte ethylene carbonate (EC), and dimethyl carbonate (DMC) in the presence of dissoluted Mn^{2+}, a paramagnetic nuclei to indirectly observe and quantify the Mn amount dissoluted into the electrolyte.

Calibration of ^{1}H MRI signal intensity with manganese (Mn^{2+}) concentration

The changes in ^{1}H MRI signal intensity in the presence of paramagnetic Mn^{2+} were validated using gel electrolyte (1 M lithium hexafluorophosphate ($LiPF_6$) in EC:DMC + poly(vinylidene fluoride-co-hexafluoropropylene) (PVdF-HFP)) with different concentrations of $MnCl_2$ (0, 24, 48 μM). The results are shown in Fig. 1b, c, where the image contrast increases linearly with an increase in Mn^{2+} concentration. This is due to the decrease in the T_1 relaxation time of the protons in EC/DMC with increasing Mn concentration [relaxation time of the electrolyte is given in Supplementary Table 2]. A calibration was determined by linear least square fit, giving the following equation

$$Y = 3.6\,(\pm 0.23)\,x\,10^6\,X + 53.547\,(\pm 7) \quad (2)$$

The result indicated that we could detect manganese ions in the order of μM.

Earlier reports have shown that MRI images are strongly affected by the presence of local magnetism from the electrode materials and metals used in batteries[16,22]. Therefore, we have investigated the effect of current collectors and cathode material on the MR images. The schematic diagram of the homemade cell used for the in-situ ^{1}H MRI measurement is shown in Supplementary Fig. S1a, b. The parameters and conditions were optimized so that the images were not affected/distorted by the magnetic property of the materials used, as shown in Supplementary Fig. S2a–c. Moreover, the effect of the current under the magnetic field during in-situ measurement was studied briefly, and the results are shown in Supplementary Figs. S3 and 4).

Dissolution of Mn^{2+} in conventional electrolyte

The in-situ ^{1}H MRI measurement results for Li/LMO cell using 1 M $LiPF_6$ EC:DMC electrolyte is shown in Fig. 2(a–c). The charge–discharge profile is shown in Fig. 2a, and MR images acquired at regular intervals during charging and discharging is shown in Fig. 2b. The image acquired before

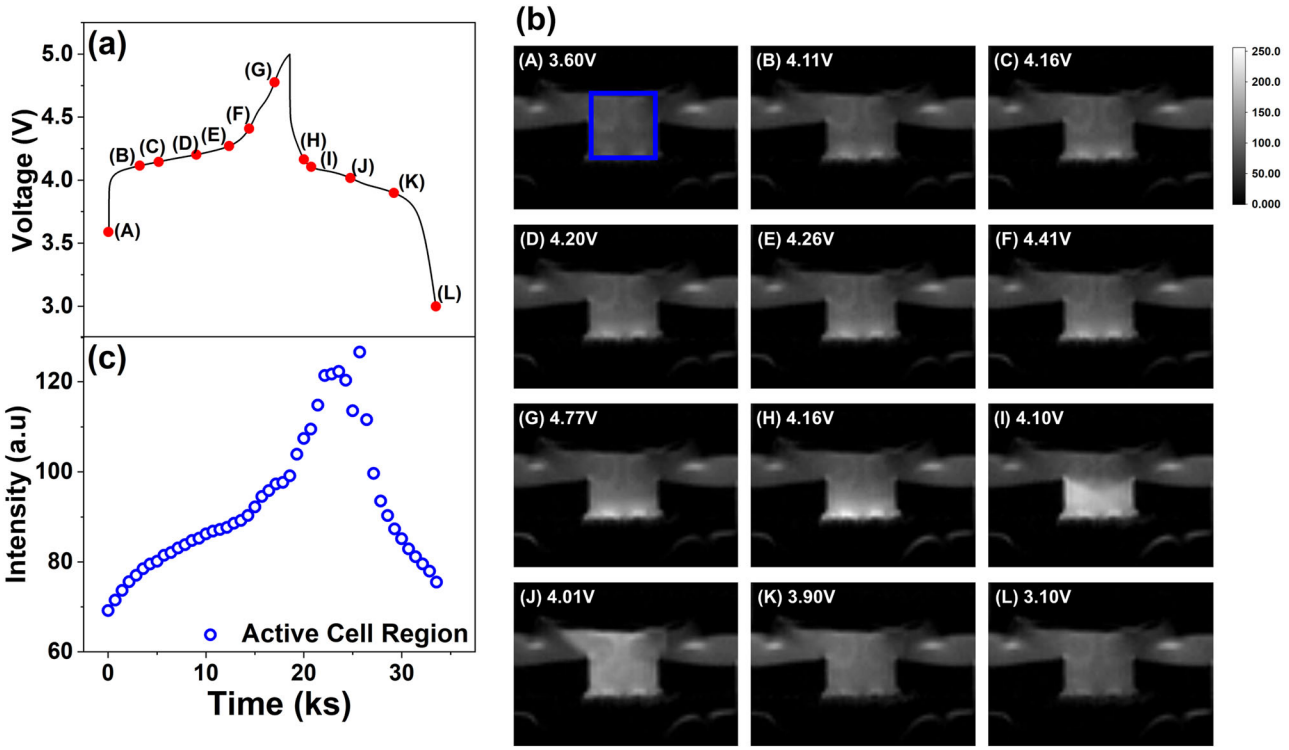

Fig. 2 | Observation of dissoluted manganese. a Charge–discharge profile for $LiMn_2O_4$/1 M $LiPF_6$ EC:DMC/Li cell, **b** ^1H MR images acquired at potentials mentioned in (**a**), and (**c**) ^1H MRI signal intensity corresponding to the active cell area (the square region between the electrodes marked in the blue frame in (**b**).

applying current (Fig. 2b(A)) shows an even distribution of the signal intensity. During charging between 4.1–4.7 V, signal intensity near the LMO cathode increases significantly, and beyond 4.7 V, a strong increase in the intensity is observed (Fig. 2b(G)). The gradual increase in signal intensity during charging indicates the presence of manganese in the electrolyte, which affects the T_1 relaxation of the solvent protons in the electrolyte (EC/DMC), leading to the increase in signal intensity (Supplementary Table 2). During discharge, the intensity near the LMO cathode spreads through the cell.

For qualitative analysis, the average MRI signal intensity was extracted and is shown in Fig. 2c. The intensity gradually increased from ~4.1 V where a plateau begins to appear (Fig. 2a). This increase in signal intensity is attributed to the presence of dissoluted manganese in the electrolyte from the LMO cathode. Although the experiments were performed in controlled atmosphere, trace amount of H_2O in the electrolyte is unavoidable, resulting in the formation of HF. During the charging process at ~4.1 V, lithium is gradually deintercalated from the LMO cathode, and a lithium-deficient phase is formed on the surface locally, which reacts with HF to form λ-Mn_2O_4 phase according to the following reaction[23] process

$$Li_{1-x}Mn_2O_4 + HF \rightarrow \lambda - Mn_2O_4 + LiF + Mn^{2+} + H_2O \quad (3)$$

where the Mn^{2+} ions get dissoluted into the electrolyte. This result corroborates with Dong et al., who reported a similar process to occur above 4.1 V[7].

Beyond 4.7 V, a rapid rise in the MRI signal intensity is observed. As charging proceeds, oxygen is released from the $Li_yMn_2O_4$ cathode (Eq. 3), leading to the oxidation of the electrolyte[24].

$$Li_yMn_2O_4 + 2\delta e^- \rightarrow Li_yMn_2O_{4-\delta} + \delta O^{2-} \quad (4)$$

When oxygen is released from $Li_yMn_2O_4$ cathode, the concentration of unstable Mn^{3+} ions increase, leading to faster and larger disproportionation of manganese ions from the LMO electrode ($2Mn^{3+} \rightarrow Mn^{4+} + Mn^{2+}$)[25–27].

Further, the MRI signal intensity increases continually and extends up to 4.1 V during discharge. This is because the manganese ions dissoluted from the surface of LMO cathode tend to accumulate in the electrolyte. Moreover, due to hydrodynamic flow of the electrolyte, the intensity spreads throughout the entire cell. After discharging the cell to lower voltages, no considerable change in the signal intensity was observed (Supplementary Movie 1).

In addition, a circular flow pattern appears near the Li anode throughout the charge–discharge cycle (Fig. 2b), which is due to the electrochemical convection in the cell[19,28]. We skip the discussion about convection phenomena here because the present article focuses on the visualization and quantification of Mn ion dissoluted from LMO cathode. The electrochemical convection affects the observed intensity profile of the manganese distribution significantly, restricting our quantitative analysis of manganese dissolution. To avoid this problem, we used a gel electrolyte consisting of 1 M $LiPF_6$ EC: DMC with PVdF-HFP polymer.

Quantification of Mn^{2+} concentration

The charge–discharge profile and MR images for the gel electrolyte system is shown in Fig. 3a, b, which shows similar behavior to that of the liquid electrolyte system. The MR images of the gel electrolyte indicate that the electrochemical convection effect observed near the lithium metal anode in the liquid electrolyte system is suppressed, which enables us to analyze the manganese dissolution into the electrolyte quantitatively. The MR images obtained at much shorter intervals are shown in Supplementary Fig. S6 and Supplementary Movie 2.

The average MRI signal intensity change with respect to charging and discharging is shown in Fig. 3c. The average intensity increases during the charging process (Fig. 3c blue circles). Like the liquid electrolyte system, above 4.1 V gradual increase in the signal intensity is observed due to the presence of dissoluted manganese[8]. Contrary to the liquid electrolyte system, during the discharging process, the MRI signal intensity does not decrease. Also, we extracted the image intensity near the cathode and is shown in Fig. 3c (red circles), where the MRI signal intensity increases till the

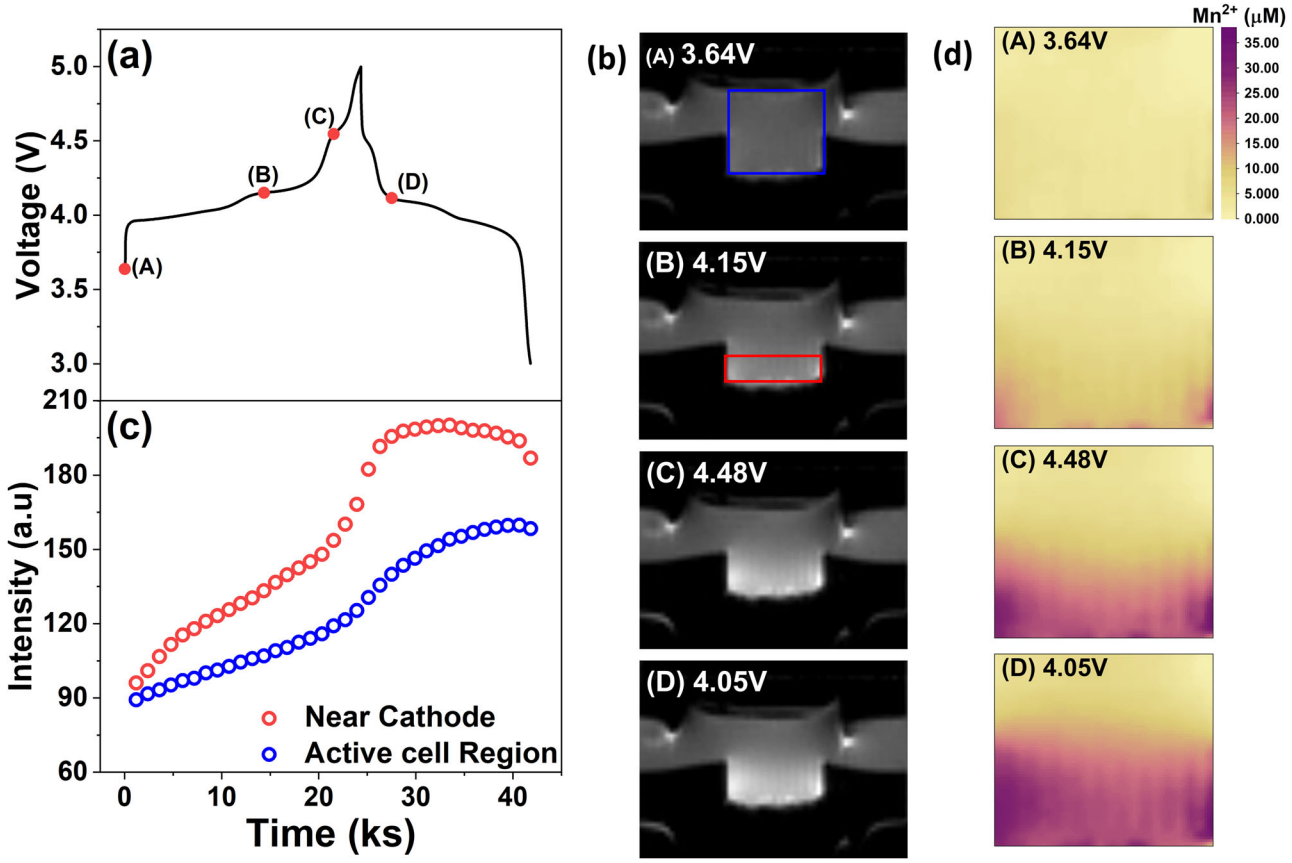

Fig. 3 | Mapping of manganese concentration. a Charge–discharge profile for LMO cell with gel electrolyte. **b** MR images acquired at potential marked in red in (**a**) and (**c**) MRI signal intensity change with respect to time extracted from the active cell region (region enclosed in the blue frame in ((**b**)(A)) and near the LMO cathode (region enclosed in the red frame in ((**b**) (B)). **d** Mn^{2+} concentration mapped images acquired at potentials indicated.

completion of the charging process and remains the same during discharging. In the absence of the electroconvection effect, the dissoluted manganese remains within the cell throughout the discharge process (Fig. 3b, c). Furthermore, manganese may be dissoluted into the electrolyte during discharge where the disproportionation reaction occurs faster. However, we cannot distinguish the contribution of manganese dissoluted during the discharge process at present.

We have converted the MR images into Mn^{2+} concentration map using the calibration curve (Fig. 1c) and shown in Fig. 3d. These maps show distribution of dissoluted Mn^{2+} ions from cathode into the electrolyte, and its propagation towards the anode. The maximum Mn^{2+} concentration estimated from the concentration map is 36 μM. To estimate the total Mn^{2+} dissoluted, we acquired MR images in the horizontal plane (XY) near the cathode, center of the cell and near the anode (Supplementary Fig. S6c, d). The amount of Mn^{2+} near the cathode, center of cell and near the anode was 28.6, 22.1, and 6.26 μM, respectively. Further, the actual volume of the region used to estimate the manganese concentration (region enclosed in blue in Supplementary Fig. S6c) near the cathode, center of the cell and near the anode was calculated to be 2.94×10^{-5} L, 2.94×10^{-5} L and 13.5×10^{-5} L respectively. Considering the actual volume estimated, the amount of manganese estimated near the cathode, center of the cell, and near the anode was found to be 8.42×10^{-10} mol, 6.51×10^{-10} mol, and 8.45×10^{-10} mol, respectively. Therefore, the total estimated amount of manganese in the cell using MRI was found to be 2.34×10^{-9} mol. Further, the amount of manganese dissoluted into the electrolyte was estimated to be 20.6×10^{-9} mol using ICP-AES measurements. The observed difference in the concentration estimated from MRI and ICP techniques is because the manganese concentration was estimated after 3 cycles using ICP, whereas the concentration from MRI is from one cycle only. Besides, the concentration estimated from both techniques falls in the same order. This demonstrates that using MRI technique metal ion dissolution in the order of few μM could be detected efficiently.

Suppression of Mn^{2+} dissolution

For comparison, the same experiment was carried out on a single solvent ether-based electrolyte methyl-3-cyanopropanoate (MCP) with lithium bis(trifluoromethane)-sulfonylimide (LiTFSI) as conductive salt[29]. The choice of new solvent and salt based on cyanoesters and LiTFSI, respectively, is to inherent high electrochemical stability and suppress HF formation[29,30]. This was expected to suppress the Mn^{2+} dissolution during the electrochemical charge–discharge process. The charge–discharge profile for $LiMn_2O_4$/1 M LiTFSI MCP/Li cell system is shown in Fig. 4a. The charge–discharge profile appears similar to that of 1 M $LiPF_6$ EC: DMC (Fig. 3a). The acquired ^1H MR images and the average MRI signal intensity for $LiMn_2O_4$/1 M LiTFSI MCP/Li cell system are shown in Fig. 4(b, c). In the case of 1 M $LiPF_6$ EC: DMC, image intensity gradually increased near the surface of $LiMn_2O_4$, indicating the dissolution of Mn^{2+} ion into the electrolyte during charging. However, in the case of 1 M LiTFSI MCP during charging, no considerable increase in image intensity was observed, indicating that Mn dissolution was suppressed in 1 M LiTFSI MCP electrolyte system (Fig. 4b, c). During discharge when the current is reversed, a slight increase in image intensity was observed, which might be due to manganese dissoluted into the electrolyte during discharge following the disproportionation of Mn^{3+} to Mn^{4+} and Mn^{2+} and the intensity being spread out of the cell due to hydrodynamic flow of the electrolyte. The image intensity change is small when compared to the gel electrolyte results, indicating that manganese dissolution is suppressed in the LiTFSI MCP system (Supplementary Movie 3).

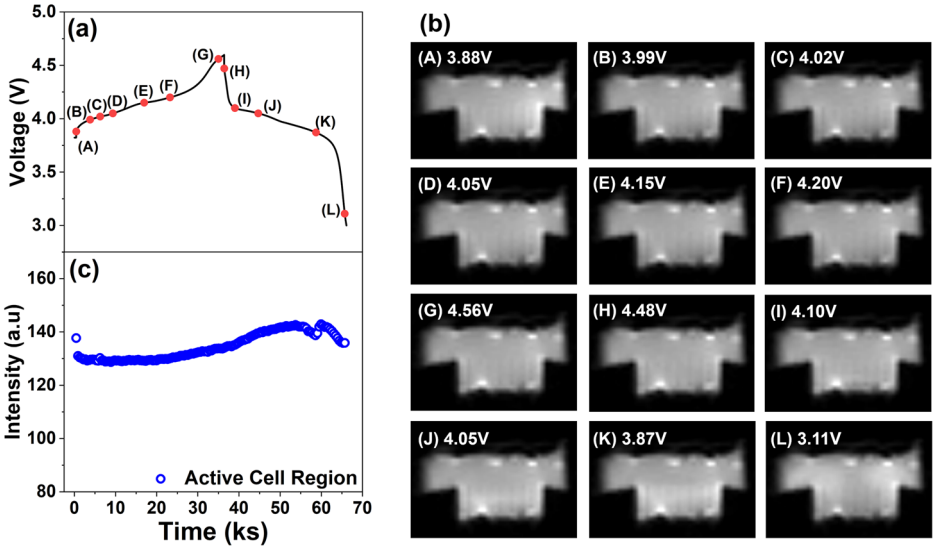

Fig. 4 | Suppression of manganese dissolution. **a** Charge–discharge profile for $LiMn_2O_4$/1 M LiTFSI MCP/Li cell, **b** ^{1}H MR images acquired at potentials mentioned in (**a**), and (**c**) ^{1}H MRI signal intensity change during charging and discharging.

Conclusions

We have illustrated a simple spin-echo technique with appreciable acquisition time to identify dissoluted Mn^{2+} in the electrolyte by ^{1}H MRI. Our results prove in-situ MRI to be a promising tool in visualizing when, where, and how Mn^{2+} dissolution occurs from $LiMn_2O_4$ electrode into the electrolyte. This approach helps in exploring the metal ion dissolution in any electrochemical systems under different electrochemical conditions, such as changing the electrolyte solution, salt, electrodes, and additives. This identification method helps to design lithium battery materials and improve their performance. In the present case, we identified an electrolyte (1 M LiTFSI MCP) that suppresses Mn^{2+} dissolution due to electrolyte oxidation during the charging process. Furthermore, MRI technique provides advantages over other techniques because it can estimate even extremely small concentration (μM) of dissoluted metal ions.

Methods

Electrode

The positive electrode was prepared by mixing $LiMn_2O_4$ (Aldrich) as an active material, PVdF (Wako Pure Chemical Industries, Ltd.) as a binder, and acetylene carbon black (Wako Pure Chemical Industries, Ltd.) at a mass ratio of 85:9:6 using N-Methyl-2-Pyrrolidone NMP (Kishida Kagaku) as a solvent. The prepared slurry was coated on the aluminum foil with a thickness of 50 μm. Care was taken to obtain uniform active material of thickness 75 μm. The active electrode material was dried at 80 °C and pressed at 40 MPa for 5 min, and the total thickness of the electrode was 59 μm.

Liquid electrolyte

In the present study, two types of electrolytes were investigated (1) 1 M $LiPF_6$ EC:DMC (1:1 v/v) (Kishida chemical co.) and (2) 1 M LiTFSI MCP. The MCP sample was received from MEET Battery Research Center, Münster, Germany.

Gel electrolyte

The gel electrolyte was prepared by dissolving PVdF-HFP (KYNAR FLEX 2801-00) in 1 M $LiPF_6$ EC:DMC (1:1) with a stoichiometry of 30 mg/L at 353 K.

In-situ MRI cell

The specially designed homemade experimental cell used for in-situ MRI measurements is shown in Supplementary Fig. S1. The cells for the in-situ MRI measurements were assembled in a controlled argon atmosphere with the dewpoint of −88 °C. The LMO cathode and the Li metal anode (0.1 mm thickness and 10 mm diameter) were separated by a hollow cylindrical spacer made of PEEK with an inner diameter and thickness of 5 mm. For safety concerns of the battery operation, a groove was introduced in the spacer, which acts as a vent for gas/bubbles to escape. For electrical contact, Pt and teflon-coated Cu wire were used on the LMO positive and Li-negative electrodes, respectively.

Electrochemical measurement

The galvanostatic charging and discharging was carried out using Toho Giken PS–08 potentiostat/galvanostat instrument at a constant current of ±25 μA in both the liquid and gel electrolyte systems.

Nuclear magnetic resonance imaging (MRI)

The ^{1}H NMR imaging measurement was carried out using Bruker Avance–400 NMR spectrometer operating at 9.4 T. A triple-axis gradient probe with vertical sample loading is used for the ^{1}H NMR imaging. The two-dimensional ^{1}H MR images were acquired using spin-echo pulse sequence. In-situ MR images were acquired with a slice thickness of 1.48 mm, size 30 × 30 mm and, a spatial resolution of 234 μm. The acquisition parameters such as echo time and repetition time were fixed as 9.0 and 500 ms for the 1 M $LiPF_6$ EC:DMC system. For the gel electrolyte system TE and TR were fixed as 9.0 and 1000 ms respectively. For 1 M LiTFSI MCP electrolyte system TE and TR were fixed as 10.4 and 500 ms, respectively. The number of integration times (NS) was four. The minimum acquisition time to obtain a single image was 4 min 16 s. The open-source ImageJ software was used for further analysis of the images. All the measurements were performed at 20 °C.

Inductively coupled plasma atomic emission spectroscopic (ICP-AES) measurements

To quantitatively determine the dissoluted manganese concentration, a cell similar to that for in-situ MRI measurement was constructed and galvanostatiscally charged and discharged under similar conditions. After completing three cycles, the electrolyte was collected and the dissoluted manganese concentration was examined using Perkin Elmer's Optima 3300XL inductively coupled plasma (ICP) emission spectrometer.

Received: 19 September 2024; Accepted: 6 January 2025;
Published online: 13 February 2025

References

1. Thackeray, M. M. & Amine, K. $LiMn_2O_4$ spinel and substituted cathodes. *Nat. Energy* **6**, 566 (2021).
2. Wen, S. J. et al. FTIR spectroscopy of metal oxide insertion electrodes: a new diagnostic tool for analysis of capacity fading in secondary Li/$LiMn_2O_4$ cells. *J. Electrochem. Soc.* **143**, L143–L146 (1996).
3. Arora, P., White, R. E. & Doyle, M. Capacity fade mechanisms and side reactions in lithium-ion batteries. *J. Electrochem. Soc.* **145**, 3647–3666 (1998).
4. Nishi, Y. Lithium ion secondary batteries; past 10 years and the future. *J. Power Sources* **100**, 101–106 (2001).
5. Jang, D. H. & Oh, S. M. Electrolyte effects on spinel dissolution and cathodic capacity losses in 4V $Li/Li_xMn_2O_4$ rechargeable cells. *J. Electrochem. Soc.* **144**, 3342–3348 (1997).
6. Wang, L. F., Ou, C.-C., Striebel, K. A. & Chen, J. S. Study of Mn dissolution from $LiMn_2O_4$ spinel electrodes using rotating ring-disk collection experiments. *J. Electrochem. Soc.* **150**, A905–A911 (2003).
7. Jang, D. H., Shin, Y. J. & Oh, S. M. Dissolution of spinel oxides and capacity losses in 4 V $Li/Li_xMn_2O_4$ cells. *J. Electrochem. Soc.* **143**, 2204–2211 (1996).
8. Doh, C. H., Lee, J.-H., Lee, D. J., Jin, B.-S. & Moon, S. I. The quantitative analyses of the dissolved manganese in the electrolyte of $Li/LiMn_2O_4$ cell using by ion chromatography. *Bull. Korean Chem. Soc.* **30**, 2429–2432 (2009).
9. Gilbert, J. A., Shkrob, I. A. & Abraham, D. P. Transition metal dissolution, ion migration, electrocatalytic reduction and capacity loss in lithium-ion full cells. *J. Electrochem. Soc.* **164**, A389–A399 (2017).
10. Allen, J. P., O'Keefe, C. A. & Grey, C. P. Quantifying dissolved transition metals in battery electrolyte solutions with NMR paramagnetic relaxation enhancement. *J. Phys. Chem. C.* **127**, 9509–9521 (2023).
11. Chandrashekar, S. et al. 7Li MRI of Li batteries reveals location of microstructural lithium. *Nat. Mater.* **11**, 311–315 (2012).
12. Klett, M. et al. Quantifying mass transport during polarization in a Li ion battery electrolyte by in situ 7Li NMR imaging. *J. Am. Chem. Soc.* **134**, 14654–14657 (2012).
13. Britton, M. M., Bayley, P. M., Howlett, P. C., Davenport, A. J. & Forsyth, M. In situ, real-time visualization of electrochemistry using magnetic resonance imaging. *J. Phys. Chem. Lett.* **4**, 3019–3023 (2013).
14. Chang, H. J. et al. Correlating microstructural lithium metal growth with electrolyte salt depletion in lithium batteries using 7Li MRI. *J. Am. Chem. Soc.* **137**, 15209–15216 (2015).
15. Bray, J. M., Davenport, A. J., Ryder, K. S. & Britton, M. M. Quantitative, in situ visualization of metal-ion dissolution and transport using 1H magnetic resonance imaging. *Angew. Chem. Int. Ed.* **55**, 9394–9397 (2016).
16. Ilott, A. J., Mohammadi, M., Chang, H. J., Grey, C. P. & Jerschow, A. Real-time 3D imaging of microstructure growth in battery cells using indirect MRI. *Proc. Natl Acad. Sci. USA* **113**, 10779–10784 (2016).
17. Romanenko, K., Jin, L., Howlett, P. & Forsyth, M. In situ MRI of operating solid-state lithium metal cells based on ionic plastic crystal electrolytes. *Chem. Mater.* **28**, 2844–2851 (2016).
18. Tang, M. et al. Following lithiation fronts in paramagnetic electrodes with in situ magnetic resonance spectroscopic imaging. *Nat. Commun.* **7**, 13284–13291 (2016).
19. Dorai, A., Kawamura, J. & Omata, T. Visualization of polysulfide dissolution in lithium-sulfur batteries using in-situ NMR microimaging. *Electrochem. Commun.* **141**, 107360–107369 (2022).
20. Dorai, A., Panigrahi, M., Iwai, Y., Hellar, N. & Kawamura, J. Magnetic resonance imaging: an innovative approach to observe rare metal extraction using ionic liquid. *Phys. Chem. Chem. Phys.* **26**, 18021–18029 (2024).
21. Iwai, Y. & Kawamura, J. Observation of electrophoretic nuclear magnetic resonance imaging in polymer electrolyte. *J. Phys. Soc. Jpn.* **79**, 160–162 (2010).
22. Ohno, D., Iwai, Y. & Kawamura, J. Nuclear magnetic resonance imaging of Li-ion battery. *Atom Indones.* **36**, 129–132 (2010).
23. Vetter, J. et al. Ageing mechanisms in lithium-ion batteries. *J. Power Sources* **147**, 269–281 (2005).
24. Gao, Y. & Dahn, JR. Correlation between the growth of the 3.3 V discharge plateau and capacity fading in $Li_{1+x}Mn_{2-x}O_4$ materials. *Solid State Ion.* **84**, 33–40 (1996).
25. Terada, Y., Nishiwaki, Y., Nakai, I. & Nishikawa, F. Study of Mn dissolution from LiMn2O4 spinel electrodes using in situ total reflection X-ray fluorescence analysis and fluorescence XAFS technique. *J. Power Sources* **97-98**, 420–422 (2001).
26. Leung, K. First-principles modeling of the initial stages of organic solvent decomposition on $Li_xMn_2O_4$(100) surfaces. *J. Phys. Chem. C.* **116**, 9852–9861 (2012).
27. Benedek, R. Role of disproportionation in the dissolution of Mn from lithium manganate spinel. *J. Phys. Chem. C.* **121**, 22049–22053 (2017).
28. Nakabayashi, S., Inokuma, K. & Karantonis, A. Magnetic effect for electrochemically driven cellular convection. *Phys. Rev. E* **59**, 6599–6608 (1999).
29. Brox, S. et al. Alternative single-solvent electrolytes based on cynoesters for safer lithium-ion batteries. *ChemSusChem* **9**, 1704–1711 (2016).
30. Brox, S. et al. Innovative, non-corrosive LiTFSI cyanoester-based electrolyte for safer 4 V lithium-ion batteries. *ChemElectroChem* **4**, 304–309 (2017).

Acknowledgements

This work was supported by the Research and Development Innovative for Scientific Innovation of New Generation Battery (RISING) project from New Energy and Industrial Technology Development Organization (NEDO), Japan. One of the authors, S. B. is grateful to the Japan Society for the Promotion of Science (JSPS) for the Post-Doctoral Research Fellowship (Grant Number: [PE-17701]).

Author contributions

N.H. and Y.I. contributed equally to this work. J.K. conceived the project idea. N.H., Y.I., M.O., and S.B. performed the experiments, analyzed and interpreted with A.D., R.T., N.K., and J.K. J.K. and M.W. supervised the work. All authors contributed to the writing of the manuscript. All authors have given approval to the final version of the manuscript.

Competing interests

The authors declare no competing interests.

Additional information

Supplementary information The online version contains supplementary material available at https://doi.org/10.1038/s43246-025-00733-2.

Correspondence and requests for materials should be addressed to Nithya Hellar or Junichi Kawamura.

Peer review information *Communications materials* thanks Yu Qiao, Bingwen Hu, and the other, anonymous, reviewer(s) for their contribution to the peer review of this work. Primary handling editors: Guangmin Zhou and Jet-Sing Lee. A peer review file is available.